

Analysis of Flapping Mechanism for Acoustically Actuated Microrobotics

Christopher House¹, Jenelle Piepmeier¹, John Burkhardt¹, Samara Firebaugh¹

¹US Naval Academy, 101 Buchanan Road, Annapolis, MD, USA 21402

Email: m143024@usna.edu, piepmeie@usna.edu, burkhard@usna.edu, firebaug@usna.edu

Abstract — The field of microrobotics has vast applications including non-invasive surgery, targeted drug delivery, and telemetry. Many groups are developing or have developed magnetically based actuation methods for microrobotics. These magnetically based systems can potentially lead to undesirable effects on the human body. Acoustic control provides an interesting alternative to existing magnetic or electrostatic actuation in that acoustic signals include few harmful effects on the human subject. Furthermore, the use of acoustic signals allow for the possibility to leverage existing medical imaging technology. This paper describes an alternative method of actuation which utilizes double-jointed, flagella-like, flappers designed for whip-like, non-reciprocal motion. The flapper mechanism was investigated using COMSOL Multiphysics finite element software to determine eigenfrequencies. Flappers were then constructed from laser cut acrylic and styrene and joined with plastic cement. The flappers were excited to resonance and displayed behavior that was consistent with simulation. A 130 mm x 50 mm x 0.2 mm robot with the flapper tail was then constructed and tested in a tank containing water and an underwater speaker. The robot exhibited forward velocities as high as 2.5 mm/s as well as frequency selectivity, which could be exploited to achieve steering in the future by using multiple flappers with different resonance frequencies. This project lays the foundation for the development of an acoustically actuated microscale robot.

Index Terms - Microrobotics, COMSOL, non-reciprocal motion, low Reynolds number, swimming microrobots, microrobotic propulsion

I. INTRODUCTION

With the end goal of medical applications such as non-invasive surgery and targeted drug delivery, an acoustically driven resonant structure is proposed for microrobotic propulsion. Many groups have developed microrobotic propulsion systems using electromagnetic power delivery systems [1]-[5]. Sonic and ultrasonic means of power delivery are an intriguing alternative because of their potential leverage of preexisting medical technology and greater safety. Denisov and Yeatmen have used ultrasonic energy transfer to microstructures with success [6], and Wang *et al.* have demonstrated propulsion of metallic microrods with ultrasonic waves [7].

A challenge with propulsion at the microscale is that this is a low Reynolds number environment; propulsion requires non-reciprocal motion from the robotic structure [8]; thus, a “flapper” with multiple, flexible joints, has been designed to produce excitation modes that involve the necessary flagella-like bending for non-reciprocal motion.

II. DESIGN

A key issue in designing a swimming microrobot is its propulsion system. The Reynolds number, a measure of the effect of inertial forces over viscous forces, is used to classify the flow regime for different systems. It is given by:

$$Re = \frac{\rho \cdot v \cdot L}{\mu} \quad (1)$$

Where ρ is the density, v is the velocity, L is the characteristic length of the object and μ is the dynamic viscosity. Microscale objects moving in water or similar fluids typically have very low Reynolds numbers, of the order of 0.1 or less.

For $Re \ll 1$, the characteristic fluid flow develops into Stokes’ Flow, also called “creeping flow,” due to the very slow nature of the fluid flow around the object. A comparable analogy to Stokes’ Flow is for a human to attempt to swim through a pool of molasses. For such a low Reynolds Number, the inertial forces acting on the submerged object are essentially negligible. The drag force on a submerged object is proportional to its velocity, and furthermore, the object can only move by the action of external forces. This requires non-reciprocal motion [8] to effect a forward velocity.

To achieve this, a two-jointed flapper (Fig. 1) was designed in which one joint was designed to bend asymmetrically. This allows for the second mass and joint to bend in a manner similar to a whale or dolphin’s “kick” at the bottom of their stroke, resulting in forward thrust for the entire structure.

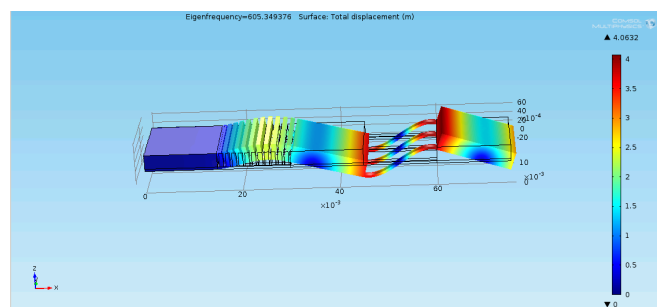


Figure 1: COMSOL simulation of an eigenmode of the flapper. Note the necessary double bend needed for non-reciprocal motion.

While the eventual goal is to scale the flapper down to microscale dimensions, initial prototyping was done at a larger scale to allow for rapid fabrication and testing. Table I shows a comparison of Reynolds numbers for different scale sizes of robots submerged in different fluids. While the eventual goal for this work is a microscale robot that would operate in water, the use of more viscous fluids would allow for a milli-scale robot to operate in the same fluid regime.

TABLE I
COMPARISON OF REYNOLDS NUMBERS FOR DIFFERENT
ROBOT SCALES

Robot Scale	Fluid	L (m)	ρ (25°C) (kg/m ³)	ν (m/s)	μ (25°C) (Pa·s)	Re
Micro	Water	100×10^{-6}	997	1×10^{-3}	8.90×10^{-4}	0.1120
Milli	Water	1×10^{-3}	997	0.1	8.90×10^{-4}	112.0225
Milli	Honey	1×10^{-3}	1360	0.1	0.4	0.3400
Milli	Castor Oil	1×10^{-3}	960	0.1	0.65	0.1476

The proposed flapping structure was initially modeled with a lumped parameters model of three masses and two springs (functioning as flexible joints). A 3-D model was developed and implemented in COMSOL, and analyzed to determine the structure's natural frequencies and mode shapes. The results of the COMSOL model confirmed that the proposed model would be capable of achieving the necessary bending modes for non-reciprocal motion

III. FLAPPER FABRICATION AND TESTING PROCEDURE

A. Fabrication

The milliscale flapper was fabricated out of acrylic and styrene using a laser cutter. The fabrication process started with the styrene frame and acrylic “mass” sections being cut into specific designs with the laser cutter. The acrylic mass sections were then bonded to the styrene frame using plastic cement. The first flapper iteration (Fig. 2) consisted of a 45 mm x 15 mm x 0.2 mm cutout of styrene, with two 15 mm x 15 mm x 0.8 mm acrylic sections.

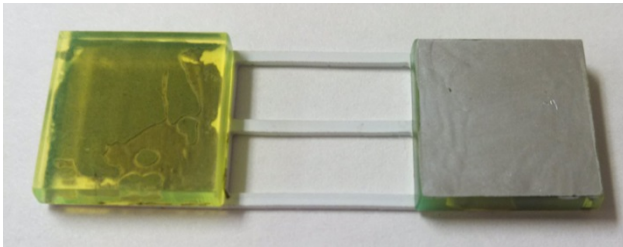


Figure 2: First flapper iteration (45 mm x 15 mm x 1.0 mm)

The second flapper iteration (Fig. 3) was fabricated in the same manner as the first flapper design with an extra step to include the grooves added to achieve non-reciprocal modes. The 75 mm x 15 mm x 0.2 mm styrene frame and 15 mm x 15 mm x 0.8 mm acrylic sections were cut with the laser cutter and bonded using plastic cement. The grooves were then cut to a very fine precision and bonded to the flapper in the same manner.

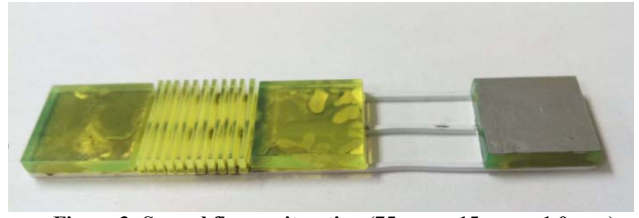


Figure 3: Second flapper iteration (75 mm x 15 mm x 1.0 mm)

B. Testing Procedure

Initial tests of the flapper used a mechanical shaker as the excitation source and a fiber optic displacement sensor for measuring the response of the flapper. The anchoring of the flapper, shown in Fig. 4, insured good coupling between the shaker and flapper.

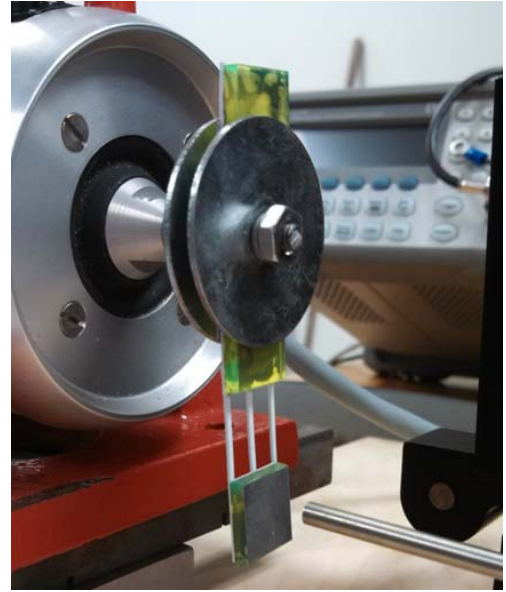


Figure 4: The mechanical shaker, first flapper design, and fiber optic sensor.

In order to determine the response of the flapper, the fiber optic sensor was calibrated so that the input signal could be swept over a range of frequencies and the sensor would subsequently measure the displacement of the unfixed end of the flapper using reflectance. One issue with the flappers was that the acrylic mass sections did not initially reflect enough light to obtain a good response signal with the fiber optic sensor. Thus, the flapper ends were coated with lustrous silver paint, as shown in Fig. 2.

IV. FLAPPER RESULTS

Tests confirmed that the proposed flapper design's behavior matched COMSOL predictions of natural frequencies. Specifically, modes were witnessed at with spacing very close to the predicted values, as shown in Tables II and III. Table II describes the results for the single-jointed flapper and Table III describes the results for the double-jointed flapper.

TABLE II
COMPARISON OF MODEL AND MEASURED RESONANCE FREQUENCIES FOR
SINGLE-JOINTED FLAPPER

Actual Eigenfrequencies (Hz)	Ratio to First Mode	Expected Mode shape	Expected Eigenfrequencies (Hz)	Ratio to First Mode	Actual Mode Shape
25	1.0	Bending	36.40	1.0	Bending
150	6.0	Twisting	202.59	5.6	Twisting
190	7.6	Twisting	393.59	10.8	Twisting
310	12.4	Bending	456.02	12.5	Bending

TABLE III
COMPARISON OF MODEL AND MEASURED RESONANCE FREQUENCIES FOR
DOUBLE-JOINTED FLAPPER

Actual Eigenfrequencies (Hz)	Ratio to First Mode	Expected Mode shape	Expected Eigenfrequencies (Hz)	Ratio to First Mode	Actual Mode Shape
15	1.0	Bending	14.39	1.0	Bending
90	6.0	Bending (double bend)	95.17	6.6	Bending (double bend)
180	12.0	Twisting	189.75	13.2	Twisting
200	13.3	Twisting	304.78	21.2	Twisting
380	25.3	Bending (double bend)	331.03	23.0	Bending (double bend)
650	43.3	Bending (double bend)	605.35	42.1	Bending (double bend)

Figures 5 and 6 show images of the flappers at their resonance modes as captured with the high-speed camera. These results established that the flapper mechanisms were behaving as expected.

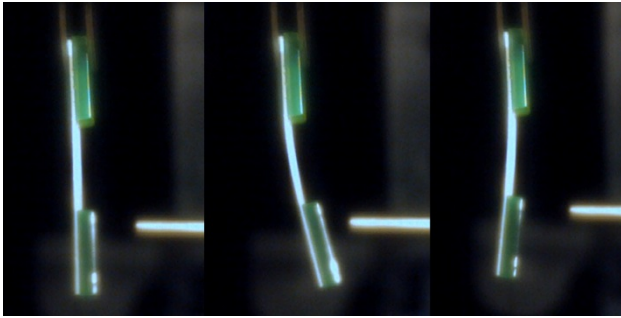


Figure 5: Images of the single-jointed flapper at its 25 Hz mode.

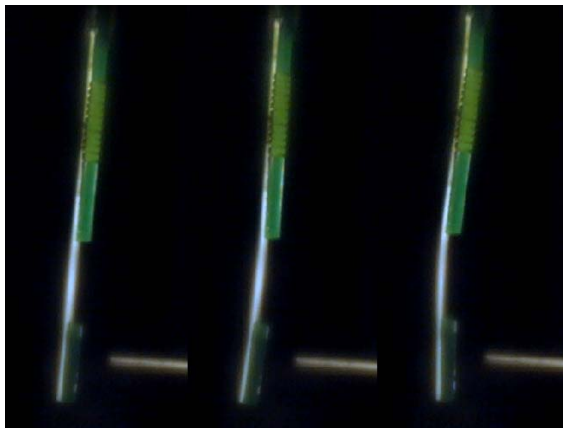


Figure 6: Images of the double-jointed flapper at its 90 Hz mode.

V. APPLICATION TO SWIMMING ROBOTS

A. Swimmer Design and Fabrication

Following confirmation of the expected and actual behavior of the flapper, a robot incorporating the double-jointed flapper was designed to facilitate propulsion while submerged. The swimming robot is shown in Fig. 7. The robot was designed so that the large body section would allow for greater coupling to the acoustic field while also allowing for forward displacement in a fluid. The robot was modeled in COMSOL to determine a rough estimate of the resonance modes as well as its behavior over several periods of motion. It was fabricated in the same fashion as the flappers.

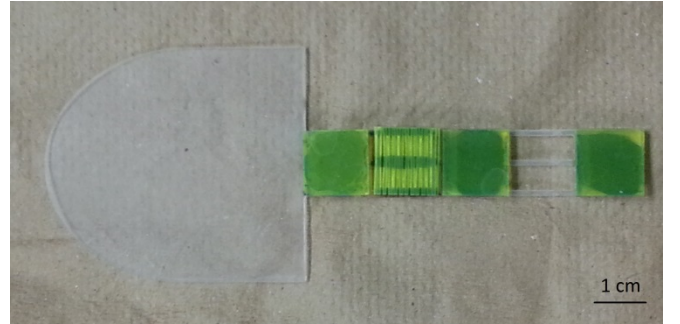


Figure 7: The swimming robot, consisting of a styrene head with the double-jointed flapper attached as a tail.

B. Fluidic Environment Testing

Following modeling and fabrication, the robot was tested within a fluidic environment. Water was used for initial testing. The test setup involved a 16"x16"x10" tank surrounded by acoustic damping foam and filled with the desired test fluid, and a 30 W underwater speaker in the center of the tank (Fig. 8). The input was controlled by a function generator and amplifier. In order to capture the motion of the robot, a camera was placed directly above the speaker. In order to constrain the vertical position of the robot, since neutral buoyancy was not attained in water, a horizontal track was set up using thin lines to support it above the speaker.

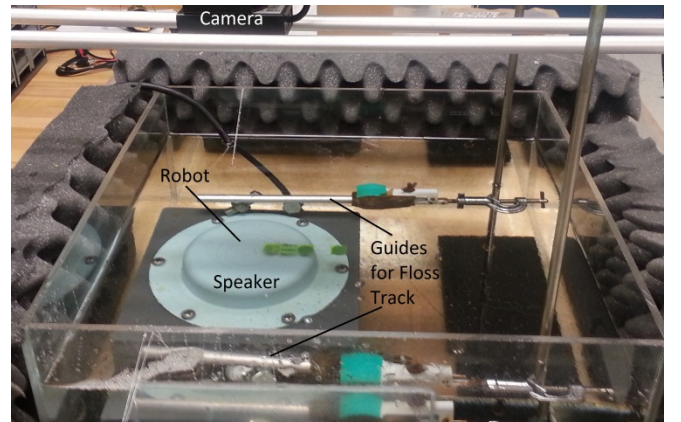


Figure 8: The fluidic environment test setup consisted of a tank with an underwater speaker attached to a function generator via an audio amplifier. A camera is suspended above the tank. A horizontal track was set up using floss to maintain the vertical position of the robot.

Following successful video capture, the data was analyzed using MATLAB®. The images captured were processed frame by frame in order to track the centroid (Fig. 9) and orientation of the robot and thus, its movement over time. This analysis allowed for the calculation of the forward velocity of the robot through the fluid.



Figure 9: Comparison of an actual video frame and the same frame processed in MATLAB to compute the centroid of the robot in order to track its position over time.

C. Swim Test Results

The robot was observed to move forward at the resonance frequency for the flapper. Fig. 10 shows the position of the centroid in pixels for a 173 Hz excitation over roughly a 20 s time period, and Fig. 11 shows the frame-to-frame forward velocity. The motion of the robot in response to the 173 Hz source is not perfectly linear but achieves clear forward motion at an average velocity of approximately 2.5 mm/s.

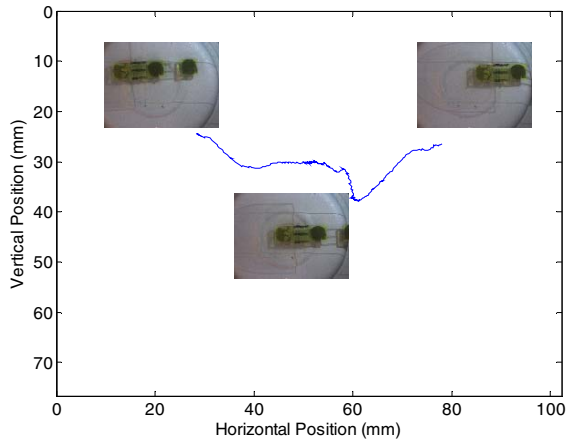


Figure 10: Robot position (in mm) at 173 Hz, showing its forward travel (from right-to-left) with corresponding frames overlaid.

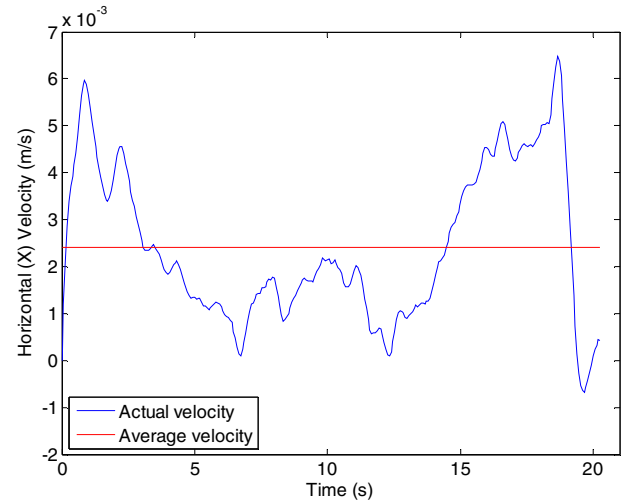


Figure 11: Robot forward velocity as function of time for excitation at 173 Hz. The average is 2.5mm/s.

Fig. 12 demonstrates the frequency selectivity of the mechanism. Like the flapper models, the robot has close agreement with COMSOL in terms of resonance mode spacing. The COMSOL model predicted eigenfrequencies approximately 115 Hz and 140 Hz, and the robot responds to inputs of roughly 140 Hz and 173 Hz. Furthermore, the lower mode was predicted to have some twisting elements as well as bending motion while the 173 Hz mode was predicted to be a purely bending mode. This is corroborated by the different average velocities, with the twisting-bending hybrid mode having a smaller velocity than the pure bending mode.

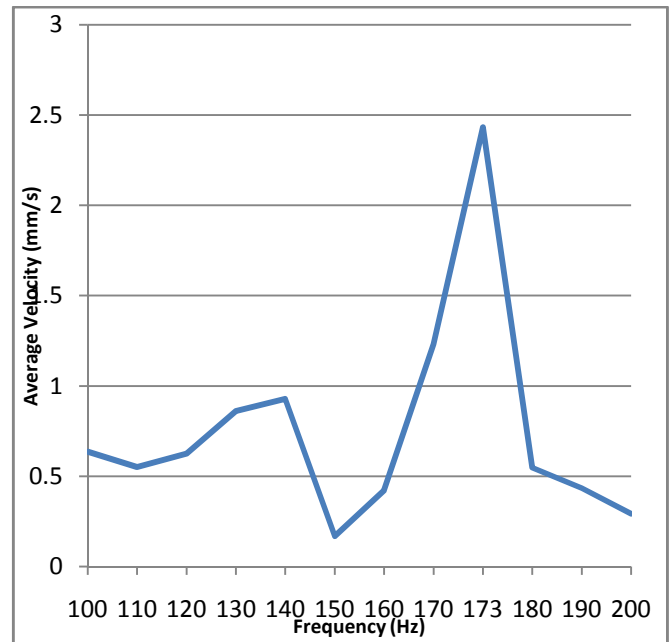


Figure 12: Robot forward velocity as function of excitation frequency.

VI. SUMMARY

A method for acoustic actuation of a swimming robot utilizing non-reciprocal motion has been proposed. Non-reciprocally moving flappers were designed and tested. These flappers were attached to a robot body which was then tested in water. This robot displayed frequency-selective forward motion. Steering could be accomplished with this mechanism by incorporating multiple flappers tuned to different resonance frequencies.

To demonstrate that this mechanism will scale down the robot will be tested next in a high viscosity fluid so that the system's Reynolds number matches that of a microrobot operating in water.

ACKNOWLEDGEMENT

This work was supported by the United States Naval Academy Trident Scholar Program, and the Program Executive Office Integrated Warfare Systems. The authors also wish to thank Prof. Brad Bishop for the use of the Gamma Lab for device fabrication, and the Technical Services Department for their support.

REFERENCES

- [1] C. Pawashe, S. Floyd and M. Sitti, "Modeling and experimental characterization of an untethered magnetic micro-robot," *Intl J Robotics Research*, vol. 28, pp. 1077-1094, 2009.
- [2] C. Pawashe, S. Floyd, E. Diller, M. Sitti, "Two-dimensional autonomous microparticle manipulation strategies for magnetic microrobots in fluidic environments," *IEEE Trans. Robotics*, vol. 28, pp. 467-477, 2012.
- [3] K. E. Peyer, L. Zhang, B. J. Nelson, "Bio-inspired magnetic swimming microrobots for biomedical applications," *Nanoscale*, vol. 5, pp. 1259-1272, 2013.
- [4] S. Schuerle, S. Erni, M. Flink, B. E. Kratochvil, B. J. Nelson, "Three-dimensional magnetic manipulation of micro- and nanostructures for applications in the life sciences," *IEEE Trans Magnetics*, vol. 49, pp. 321-330, 2013.
- [5] S. Martel, "Navigation control of micro-agents in the vascular network: challenges and strategies for endovascular magnetic navigation control of microscale drug delivery carriers," *IEEE Control Syst*, vol. 33, pp. 119-134, 2013.
- [6] A. Denisov and E. Yeatman, "Stepwise microactuators powered by ultrasonic transfer," *Procedia Engineering*, vol. 25, pp. 685-688.
- [7] W. Wang, L. A. Castro, M. Hoyos, T. E. Mallouk, "Autonomous motion of metallic microrods propelled by ultrasound," *ACS Nano*, vol. 6, pp. 6122-6132, 2012.
- [8] E. M. Purcell, "Life at low Reynolds number," *Amer. J. Phys.*, vol. 45, pp. 3-11, 1976.